PET/CT SHIELDING DESIGN COMPARISIONS

A Thesis

by

AUDRA LEE COKER

Submitted to the Office of Graduate Studies of
Texas A&M University
in partial fulfillment of the requirements for the degree of

MASTER OF SCIENCE

May 2007

Major Subject: Health Physics

PET/CT SHIELDING DESIGN COMPARISONS

A Thesis

by

AUDRA LEE COKER

Submitted to the Office of Graduate Studies of
Texas A&M University
in partial fulfillment of the requirements for the degree of

MASTER OF SCIENCE

Approved by:

Chair of Committee,	John W. Poston, Sr.
Committee Members,	Art Boyer
	John R. Ford
	Michael Walker
Head of Department,	John W. Poston, Sr.

May 2007

Major Subject: Health Physics

ABSTRACT

PET/CT Shielding Design Comparisons. (May 2007)

Audra Lee Coker, B.S., Texas A&M University

Chair of Advisory Committee: Dr. John W. Poston, Sr.

The objective of this project was to compare two different methods of calculating dose through lead-shielded walls in the PET/CT suite at Scott & White Hospital in Temple, Texas. The ultimate goal was to see which of the two methods agreed with the actual physical measurements. Minimizing shielding needed in future suite designs would result in a possible reduction of structural as well as financial burden. Formulas and attenuation coefficients following the basic January 2006 AAPM guidelines were used to calculate unattenuated radiation through existing lead walls. The computer code MCNPX was used to simulate the leaded walls of the PET/CT suite and provide another set of results. These two sets of results were compared to doses gathered from OSL badges placed around the suite for a period of two months. For this type of problem, MCNPX proved to provide results that were inconsistent and unreliable. It was concluded that the traditional computational methods are the most reliable for designing shielding in a PET/CT suite.

ACKNOWLEDGEMENTS

I would like to thank my graduate advisor, Dr. Poston, for his patience with me through the endless email questions while I worked on my thesis off-campus. I would like to thank two of my other committee members, Dr. Ford and Dr. Walker, for standing by with references and suggestions while I struggled through the process of research. Very importantly, I would also like to thank my fourth committee member, Dr. Boyer, for allowing me to use the Scott & White facility for my research: without this opportunity, my research could not have been done. Special thanks to David Jones, at Scott & White Hospital, for his assistance throughout my project. Most of all, I want to thank my family who, from across the country, have supported me in my decision to attend graduate school even after all the struggles as an undergraduate; and my husband Kevin, who put up with the early mornings and late nights that graduate school requires!

TABLE OF CONTENTS

LIST OF FIGURES

LIST OF TABLES

CHAPTER I

INTRODUCTION

Shielding for radiation producing equipment and sources, such as Computed Tomography (CT) and Positron Emission Tomography (PET) units, is typically designed using computational methods of 'tried and tested' equations. Although these methods have proven adequate in their results, with advanced computer technology, radiation transport can be modeled more accurately. This opens the possibility of using radiation fluence and distribution results from a computer model to design more cost and structurally effective shielding.

Exposure to ionizing radiation has the potential to be harmful and, in some cases, even deadly. Significant effects of radiation have been documented at high doses, but at lower doses, much of the "theory" is all speculation (Upton 2001). Most commonly, the Linear Non-Threshold (LNT) hypothesis is accepted in the field of radiation safety. The LNT hypothesis simply asserts that health detriment is linearly proportional to radiation dose with no threshold.* This brings importance to a concept of radiation safety called ALARA-- As Low As Reasonably Achievable. Because results of exposure at low levels are *not* known, the philosophy of ALARA expects that exposure rates be kept as low as possible taking into account social and economic factors (NRC 1992). As a result of the known and unknown dangers associated with radiation, lawmakers have created limits in an effort to control the doses to occupationally exposed workers. These

---

This thesis follows the style of Health Physics.

*** Poston** John W Sr. Personal communication, Texas A&M University, Department of Nuclear Engineering; 2006.

Workers have willingly accepted the risk of exposure. Dose limits are also given for the public, who are unknowingly and possibly unwillingly exposed. These limits are enforced at the federal level and sometimes the state level as well. As listed in the Nuclear Regulatory Commission's Title 10 Code of Federal Regulations Part 20 (10 CFR 20), occupationally exposed workers are not to exceed 0.05 Sv (5 rem) per year while members to the public are limited to 0.001 Sv (100 mrem) per year (NRC 1992).

Rapid leaps in technology using ionizing radiation leave challenges of ensuring the safety of the public, the patients and to the occupationally-exposed workers. There are several methods that allow exposures to be kept within the safety limits created by lawmakers. Often the installation of highly attenuating material, such as lead or concrete, within the surrounding structures (typically walls and doors), is the chosen method. Currently, computational formulas based on the attenuation coefficient of the shielding material have been used to calculate the amount of shielding needed to stay within these federal and state regulations. While the use for high-energy emitting radionuclides in the medical field (such as PET) have increased, there is evidence that calculations based on the typical narrow-beam, good-geometry attenuation coefficients may no longer provide sufficient shielding because buildup factors have been neglected. Recognition of these unacceptable attenuation coefficients dramatically changes the way shielding calculations are performed (Madsen et al 2006).

As computers become more and more integrated into our personal and work lives, their use in radiation safety programs has become more prevalent. Monte Carlo computer codes are utilized in various fields and the possibility of using these codes to determine radiation shielding requirements becomes one of these options.

This project will focus on comparing two different methods of dose calculations through lead-shielded walls in the PET/CT suite at Scott & White Hospital in Temple, Texas. The ultimate goal is to determine which of the two methods provides results that agree with the actual physical measurements of dose transmitted through the walls. The goal is to minimize the shielding needed in future suite designs, resulting in a possible reduction of structural as well as financial burden. Formulas and attenuation coefficients obtained from the basic January 2006 AAPM guidelines (Madsen et al 2006) were used to calculate unattenuated radiation through existing lead walls. The objectives of this report are as follows:

- Obtain dosimeter readings for a period of eight weeks from points of interest around the PET/CT suite;
- Calculate doses at these points of interest using formulas from the AAPM guidelines;
- Create a computer model of the PET/CT suite using a Monte Carlo code, MCNPX, and obtain dose estimates at the points of interest; and
- Compare dose calculations with the MCNPX dose results to see which method agrees with the dosimeter readings at the points of interest.

CHAPTER II

BACKGROUND

Diagnostic X-ray Imaging

Diagnostic x-ray imaging is not only a science, but also a tool that helps explore human anatomy, physiology and biochemistry. It utilizes differences in properties of the various tissues throughout the human body and employs radiation such as x rays, gamma rays and annihilation radiation to produce images that aid in diagnosing, monitoring and treating diseases (Hendee, Ritenour 2002).

Introduction of computed tomography (CT) to diagnostic imaging in the 1970's is typically recognized as the single most significant event since the discovery of x rays; transforming radiology from an analog to a digital-based specialty. Several features that make CT so useful in imaging are:

- Cross-sectional imaging of anatomy;
- Contrast resolution superior to traditional radiography; and
- Images are products of digital data, are processed by computer and can be manipulated to vary points of view.

Computed tomography is based on the basic transmission relationship shown in Equation 1:

$$I = I_o \mathrm{e}^{-\mu x} \tag{1}$$

where I is the transmission through a plane, I_o is the original source strength, μ is the voxel-specific attenuation coefficient and x is the thickness traveled through the plane. This equation assumes a monoenergetic source and a homogeneous medium. When the circumstances include a non-homogeneous medium represented by multiple, finite

volumes known as voxels, the equation changes slightly as shown in Equation 2, where the products of the average attenuation coefficient and effective thickness of each voxel are summed for each path length through which the radiation travels:

$$I = I_o e^{-\sum_{i=1}^{n} \mu_i x_i} . \quad (2)$$

With a single transmission measurement as in Equation 2, individual voxel attenuation coefficients cannot be determined. With multiple transmission measurements in the same plane but at different orientations of source and detector, multiple equations are obtained. The equations can be solved using a cross-sectional matrix of the voxel attenuation coefficients, Fourier transforms or other methods. Once obtained, attenuation coefficients from the voxels can be assigned gray levels, creating a grayscale CT image that depicts structures within the patient. A basic example of CT geometry is shown in Fig. 1.

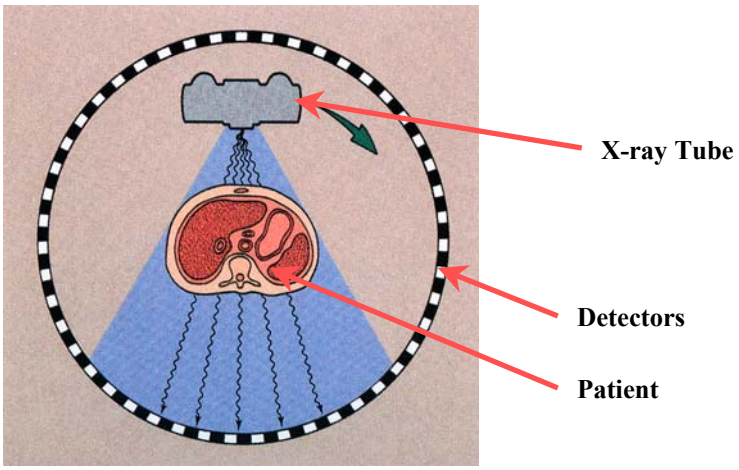

Fig. 1: CT function (with permission from Bushong 2001)

Modern CT scanners use what is called “helical” or “spiral scanning.” In this method, acquisition time is significantly decreased by transferring x-ray tube voltage through a “slip ring” that is mounted on the rotating gantry of the unit. This enables the x-ray tube to rotate in a circular motion while the patient table moves continuously through the gantry. The result is a helical, or spiral, path around the patient. Figs. 2 and 3 illustrate the process (Hendee, Ritenour 2002).

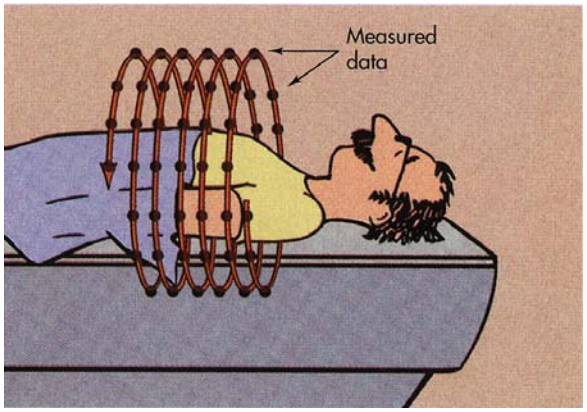

Fig. 2: The helical or spiral path around the CT patient (with permission from Bushong 2001)

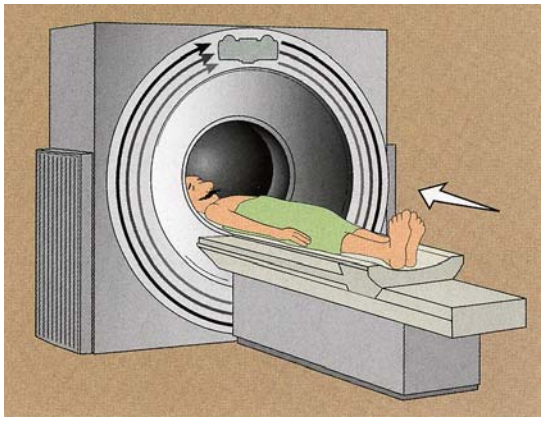

Fig. 3: A patient on the table continuously moving through the gantry (with permission from Bushong 2001).

Positron Emission Tomography (PET) is a noninvasive diagnostic imaging tool that takes advantage of certain radiopharmaceuticals and allows abnormal metabolic activity in and around organs to be examined by injection of a radionuclide into a patient (Radiology 2006). These radiopharmaceuticals, biological compounds linked to radiation-emitting radionuclides, can in some cases be tailored for concentration by a particular organ or physiologic process. As a result of the small chemical quantities administered to each patient, the radiopharmaceuticals do not disturb the physiologic processes of interest (Alazraki 1991).

PET utilizes positron-radiation to determine the radiopharmaceutical distribution within the patient. Detectors positioned around the patient detect annihilation radiation resulting from the emitted positrons interacting with electrons. The annihilation radiation is released as two 511 keV photons that are emitted 180° apart. In the event that both of these photons are detected, the origin of the decay can be localized (Hendee, Ritenour 2002).

The PET unit itself consists of a ring of detectors around the patient and through which the patient table glides. When detectors on opposite sides of the ring detect annihilation photons within 10^{-9} seconds of each other, it can be assumed that a decay took place at some point along a line between the two detectors. This concept is illustrated in Fig. 4 where Detector 1 and Detector 2 are 180° apart. The actual PET image constructed is based on the number of interactions occurring in each of the voxels, or pixels represented in the image (Hendee, Ritenour 2002).

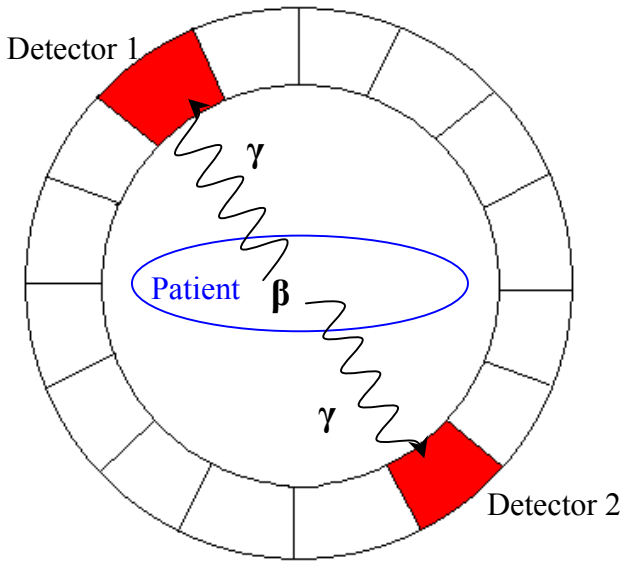

Fig. 4: How photons are detected in PET

The radiopharmaceuticals used for PET scans are typically short-lived, cyclotron-produced radionuclides that decay by positron emission (Cho et al 1993). Fluoro-2-deoxyglucose (^{18}F -FDG), a common radionuclide-bound metabolic agent used for PET in hospitals today, is a positron emitter.

When the applications of PET and CT are combined, a powerful diagnostic tool results: PET/CT. The PET portion provides molecular activity levels, while CT provides the anatomical structure of the body. CT also significantly increases the efficiency of PET by obtaining attenuation correction factors quickly, allowing for shorter scan times.

In the last five years, PET/CT has become a widely used diagnostic tool (Madsen et al 2006). The first generation of PET/CT units was a single-slice CT integrated with a

PET camera. Today's PET/CT units have a choice of up to a 64-slice CT (Siemens 2006) along with technology's most advanced detectors.

At the Scott & White facility, PET/CT patients are injected with an average of 555 MBq (15 mCi) of ^{18}F FDG and instructed to lie still in what is called the uptake room for 45-60 minutes while the radionuclide distributes throughout their body. They are then instructed to void their bladder of urine accumulation and then taken to the scan room where they are given the approximately 20-minute scan. By the time the patient leaves the PET/CT suite, the majority of the short-lived ^{18}F (half-life is 110 minutes) has either voided from their body or physically decayed.

Although this technology is very useful in the medical field today, its presence brings challenges. One such challenge is the shielding required to attenuate the high-energy photons (511 keV) being utilized. Although this procedure is for the benefit of the patient's health and may be a one-time occurrence, the technicians are exposed to the high-energy photons for a possible 40-hours per week. There are offices around the suite with non-radiation workers (physicians and staff) who may also be exposed. The solution to this problem is to design the PET/CT suite with adequate shielding to meet state and federal requirements.

The Siemens PET/CT unit used at Scott & White Hospital has a maximum energy of 140-kVp (the peak energy of a polyenergetic x-ray spectrum). The tenth value layer (TVL) of 140-kVp x rays is less than 0.95 mm. This means that when 0.95 mm of lead is placed in the beam of 140-kVp x rays, the transmission through the lead wall will be 1/10 of the initial beam strength (Bushong 2001). The annihilation photons being released from the F-18 administered to PET/CT patients have an energy of 511 keV.

The TVL of 511-keV photons is approximately 16.6 mm. This is a ratio of approximately 17:1. However it is not just the TVL that is important in determining if the shielding designed for the PET portion of the suite will adequately shield the CT portion as well—another key factor is the fluence rate. The CT portion of the unit has a much higher fluence rate than does the radiopharmaceutical distributed throughout the patient. There is about a 72 mR exposure from CT per patient while only about 0.6 mR exposure from the radiopharmaceutical per patient in the scanroom (ratio of 120:1). It is safe to assume that if the PET/CT suite is shielded for the 511-keV photons decaying in the patient, the suite will be shielded adequately for the high fluence rate of lower-energy x rays coming from the CT portion of the unit as well.

Dosimeters

Dosimeters are devices capable of providing a measurement in its sensitive volume that can be converted to absorbed dose.

Thermoluminescence dosimeters (TLD) consist of a crystalline dielectric material that contains activators allowing it to act as a thermoluminescent phosphor. The activators contain two different types of imperfections known as “traps” and “luminescence centers.” The first set of imperfections are known as electron traps and “holes”, which capture and hold charge carriers in an electric potential for a lengthy period of time. The second type of imperfection is the luminescent centers which are located at either the electron-traps or hole-traps and function as a light emitter when the electrons and holes recombine during a stimulation process using either heat (TLD) or laser light (optically stimulated luminescence, OSL). This light is measured with a photomultiplier tube. The emitted light is proportional to the radiation energy deposited

in the detector (Attix 2004). Fig. 5 illustrates the luminescence process. An ionization event elevates an electron into the conduction band where it migrates to an electron-trap. The hole that is left behind migrates to a hole-trap. At a later time when heating or laser stimulation occurs, the electron may be liberated first (although it is also possible that a hole may be released first), enters the conduction band and migrates to a hole-trap or luminescence center. This recombination is accompanied by the release of a photon of light.

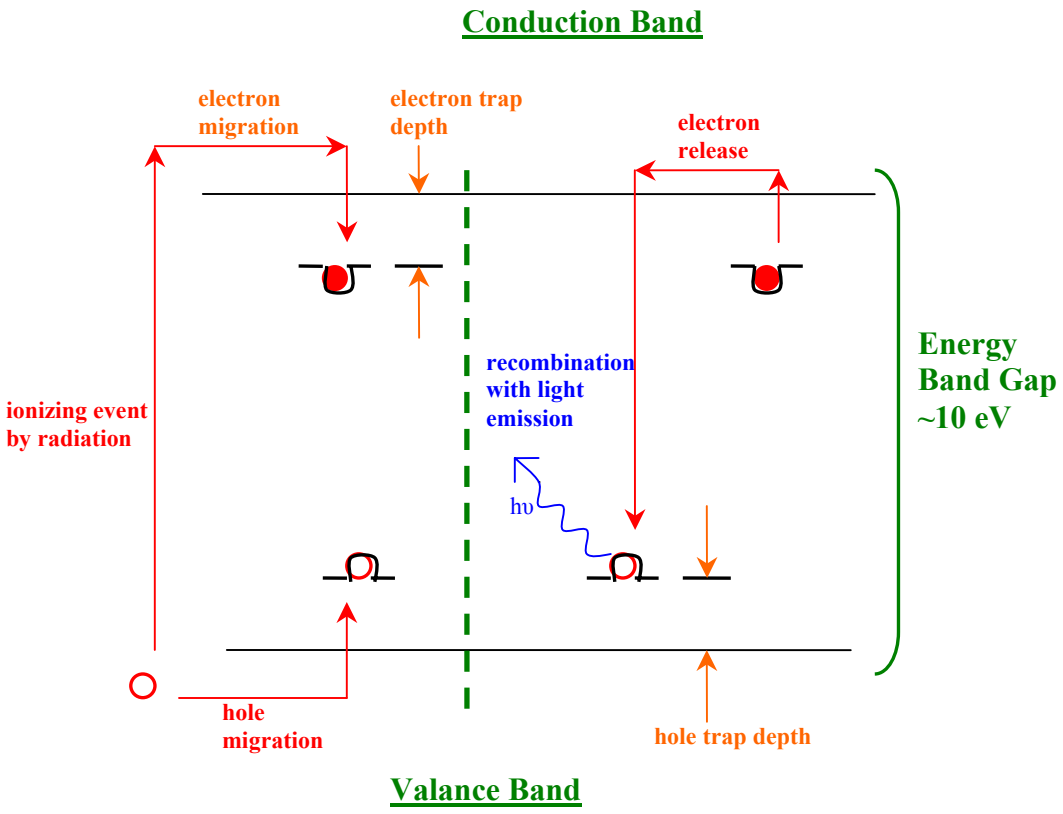

Fig. 5: A representation of the luminescence (Attix 2004)

Optically stimulated luminescence detectors are similar to TLDs: materials that emit optically stimulated luminescence are thermoluminescent as well. The difference between the two is the mechanism used to release the ions from the traps. Optically stimulated luminescent dosimeters emit their light after being stimulated by a laser in contrast to the heating process of the TLD (Frame 2004). The x- and gamma-ray dosimeters that Landauer provides contain a strip of Al_2O_3:C which is sandwiched between a three-element filter pack and sealed in light-tight material (Landauer 2005). Al_2O_3:C is produced under conditions that create defects in the crystalline structure due to missing oxygen atoms. As with TLDs, electrons become trapped in the defects of the crystalline structure. When the Al_2O_3:C is exposed to the stimulating luminescence, the electrons that are freed from the traps move to the recombination centers where light photons are released (Frame 2004).

Landauer, a longtime provider of radiation dosimeters, produces and distributes Al_2O_3:C badges including those used to physically measure exposures in the PET/CT suite at Scott & White hospital. Landauer claims that light leakage in its Luxel badges are eliminated due to the containment surrounding the active components. The Al_2O_3:C dosimeters are said to give accurate readings between 0.001 and 100 rem and can detect energies between 5 keV and 40 MeV (Landauer 2005).

Monte Carlo Techniques

The computational method known as Monte Carlo (MC) began years ago—in the late 1940's at Los Alamos National Laboratory in New Mexico. Mathematician Stanislaw Ulam realized that the then new accessibility to a computer could make

statistical sampling a practical tool (Hendricks, 1994). As a result, a program was developed to follow a large number of individual neutrons as they were scattered, caused fission, escaped or absorbed. At each stage in the life of a neutron, decisions would be made based on statistical probabilities corresponding to physical and geometric factors. Particles would be followed and processes repeated until a statistically valid picture was generated (Metropolis 1987).

The possibilities of being able to simulate a problem using a computer, without having to physically perform potentially hazardous experiments, make MC codes very powerful in the world of ionizing radiation. MC codes are advantageous in a wide range of areas in and out of the direct spotlight of nuclear technology. MC codes have been applied to areas such as criticality safety regarding nuclear weapons, waste storage sites, and fuel-fabrication. The codes are also used today in the medical field as well as nuclear safeguards field. They have been utilized in fusion research, space exploration, and even in fields not typically thought of as using nuclear technology, such as oil-well logging (Hendricks 1994).

Since the time of the first MC code, multiple versions of it have been developed, with each new version further extending its capabilities. One of the more recent such codes is MCNPX: an "all-purpose" radiation transport code that can track nearly all particles with an almost indefinite range of energies (Pelowitz 2005).

MCNPX operation depends on a physical problem simulation. The geometry of the problem must be specifically defined along with a list of parameters for the problem, some of which include the radiation type, energy, materials, sources, and number of histories to be followed. There are various facets of the code which allow for specific

characteristics pertaining to the sources, particles, energy deposition, and tallies (detectors).

There are four sections of a MCNP code titled “cards”: the title card, cell cards, surface cards and data cards. Each of these four sections is necessary for the code to perform correctly. The title card is user specified and is simply a title by which to identify the code. The cell, surface and data cards, however, entail much more detail. The surface cards form the basis of the geometry in the model. The user specifies a surface number and geometry (e.g., plane, sphere or parallel-piped) and identifies all coordinates for that geometry. This is repeated until all structures within the model are defined.

Once the surface cards are complete, the user can move on to the data cards where the materials to be used as well as particles and source types, energies and tallies (detectors) will be specified. Each material identified in the data cards must be specified by its elemental components and the percentage of each element in the material. It is in the data cards that the user specifies what radiation type will be modeled in the code (e.g., photon, neutron, alpha, etc.) and how many histories will be followed. Source size, strength and position are also input into the data cards.

Once the surface cards are complete and the data cards in progress, the cell cards must be identified. Each cell in the cell cards is a volume composed from surfaces defined in the surface cards. For a simplistic example, if a sphere is defined as a surface in the surface cards, then there would be two corresponding cells in the cell cards: one inside the spherical surface and one outside the surface. This is illustrated in Fig. 6.

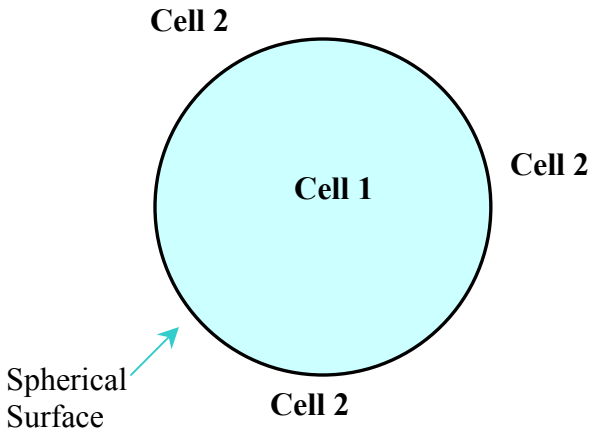

Fig. 6: An illustration of surfaces and cells.

A sample code input with a single spherical surface is shown in Fig. 7. The code has one surface card with the two cells shown in the cell cards. The sphere itself is identified to be lead with the space outside of the sphere as air.

Each cell in the cell cards contains a "cell importance." The importance of the cell is used to "push" particles to regions of interest within the geometry through various techniques. A particle history will be terminated if it enters a void cell—a cell which has no importance in the model (MCNPX Users Manual 2005).

```
Single Sphere

C_____________________________________________________________________
C Cell Cards
C_____________________________________________________________________
C Cell#  Mat#  Density      Geom       Imp
  10     1    -11.34       -1         imp:p=1  $ Inside Sphere
  20     2    -0.00120484   1         imp:p=1  $ Outside Sphere

C _____________________________________________________________________
C Surface Cards
C _____________________________________________________________________
C Surf# Name  V(x)     V(y)    V(z)    radius
  1     S     0        0       0       15

C _____________________________________________________________________
C Data Cards
C _____________________________________________________________________
C Material     ZAID         Fraction
  M1           82000.04p    1.0                $ Lead
C
  M2           6000.04p    -0.000125           $ Air
               7000.04p    -0.755267
               8000.04p    -0.231781
               18000.04p   -0.012827
 nps= 2000000
```

Fig. 7: Sample MCNPX code input.

Reliability of results is obviously one of the greatest concerns when using computer simulation to model real-life problems. MCNPX and compatible programs provide a valuable tool that aids in obtaining confidence in the results: 10 statistical checks are performed on each tally (detector). These checks are related to the following (Shultis 2004):

- Tally mean, which for the last half of the problem cannot have an upwards or downwards trend;
- Relative error, which is the ratio of the standard deviation of the tally mean to the mean, indicates the precision of the tally. The unit-less relative error must be

less than 0.1, must decrease monotonically with an increasing number of histories, *N*, as well as decrease with $1/\sqrt{N}$ for the last half of the problem;

- Variance of variance (VOV), which evaluates the accuracy of the relative error. The VOV must be less than 0.1 for tallies, decrease monotonically as well as by 1/N for the last half of the problem;
- Figure of merit, the relation of the computer execution time to relative statistical error (Hendricks, Culbertson 2000), must remain strictly constant and show no monotonic upwards or downwards trend for the last half of the problem; and
- Tally probability density function (PDF), which helps assess the quality of the confidence interval estimates for the tally mean.

Although information on the statistical analysis (created within the program) is somewhat scarce and the results are not foolproof, the statistical checks leave the user with a sense of confidence in which results to accept and which are better left rejected.

When executing Monte Carlo codes, large numbers of statistical trials are required to model how the radiation interacts with matter as a result of the randomness of the interactions. As a result, there may be a large statistical error for a given number of histories. Variance reduction is a set of techniques that allow a reduction in the statistical error by sampling more histories in regions of interest than in regions where their contributions are not desired.

Scott & White Hospital PET/CT Suite

The PET/CT suite at Scott & White Hospital houses a Siemens Biograph-16 unit. The suite provided for the PET patients consists of a hotlab, where all doses are manipulated and stored until injection time, three uptake rooms, where the patients are

injected with ^{18}F FDG; a toilet, a control room, and a scan room. Corridors and hallway surround the suite on two sides, while most of the third side consists of offices and an x-ray reading room. The back and one side of the scan room face an earthen embankment as shown in Fig. 8. The PET/CT suite is located in the basement, so there are no patients or workers below, and a lobby with a transient crowd is located above the suite.

The wall located next to the uptake room has the greatest thickness of lead in the entire suite (1.5875 cm). A lead overhang in the ceiling over the uptake rooms is meant to protect those on the first floor from any radiation that may be directed upwards. The suite is shielded from the adjacent offices with 1.25 cm of lead. The main hall in front of the suite is shielded by the same thickness of lead.[†] The reading room has an even thinner 0.635-cm slab due to the shorter occupancy time of the room. Only the door leading to the scan room is leaded solely for the purpose of shielding from the CT beam. The control room is shielded by lead on two sides for the safety of the technologists and includes a 0.3175-cm equivalent leaded-glass window to shield the room from CT. The suite was shielded to account for a maximum of ten patients per day.[†] In the sample eight-week period of this study, Landauer detectors were exposed in the suite, during which a total of 195 patients were treated. This was much less than the patient workload for which the suite shielding was designed.

[†] **Jones** David. Personal Communication, Scott & White Hospital, Department of Physics; 2006.

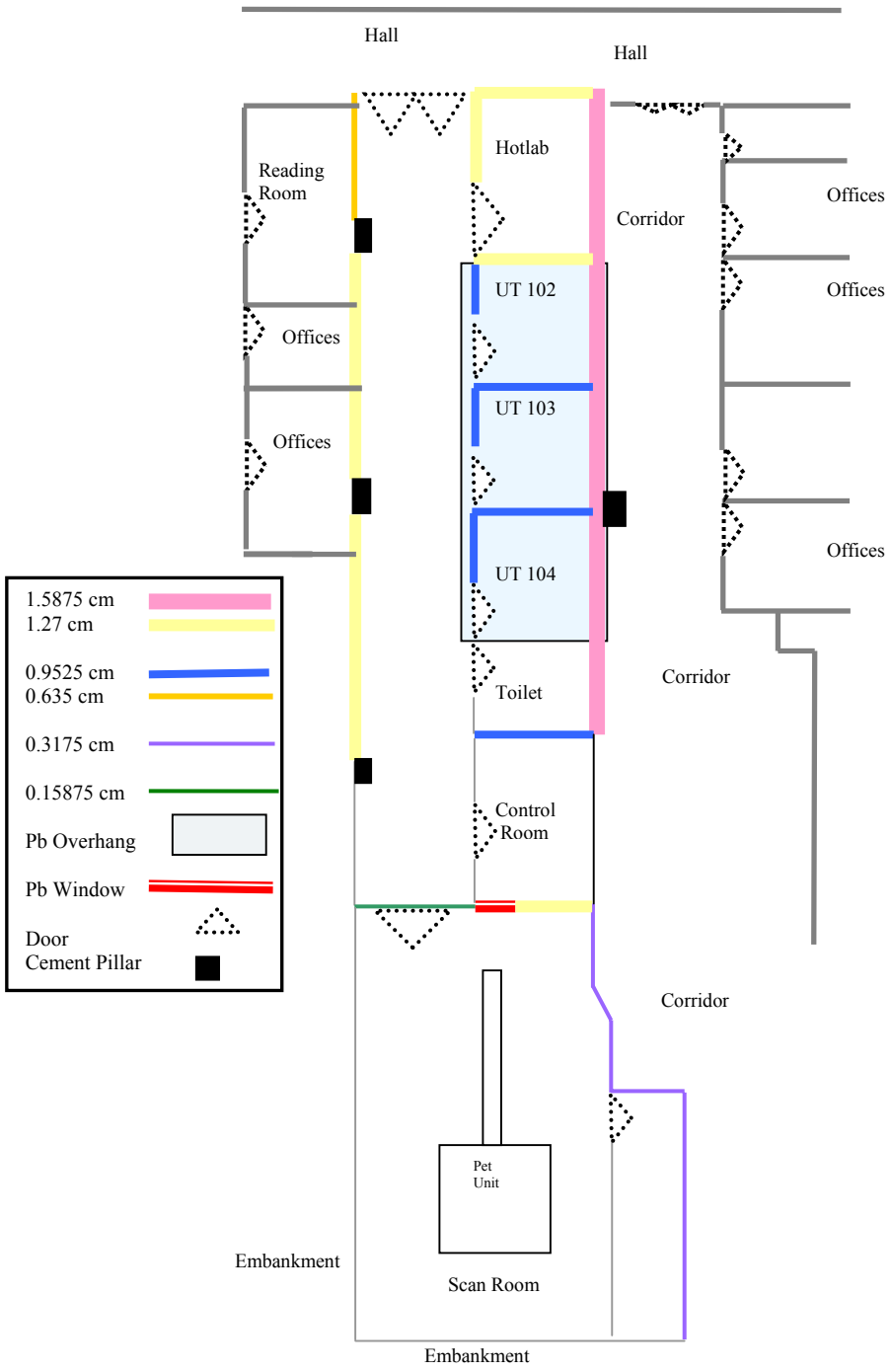

Fig. 8: The layout of the PET/CT suite at Scott & White Hospital

CHAPTER III

MATERIALS AND METHODS

Physical Measurements

The basis for comparison between computational and MC code methods is the actual, physical fluence through the lead walls. Points of interest were chosen inside as well as outside the suite and determined to be suitable places to attach a dosimeter for a period of eight weeks. The fluence through the walls from the source to dosimeter was measured by taping Landauer Al_2O_3:C x- and gamma-ray dosimeters flat against the wall with their face pointing in the direction of the sources. The dosimeters were left on the walls for a two-month period, accumulating exposure from patients within the suite. The technologists were asked to record the uptake room number for each patient as well as the activity of ^{18}F FDG administered. Unfortunately, the technologists were inconsistent in recording the number of patients in each room and so only a sample of the total patients was known. However, the total number of patients was recorded and a percentage of patients in each room was calculated. With this information, more accurate calculations could be made using both the computational and MCNPX methods. Fig. 9 is a schematic of the PET/CT suite along with the location of sources (patients) and detectors positioned around the suite. The detectors are numbered 1 through 26. Detectors 3, 4 and 6 are not included in the experiment because their intended locations were not suitable for placement.

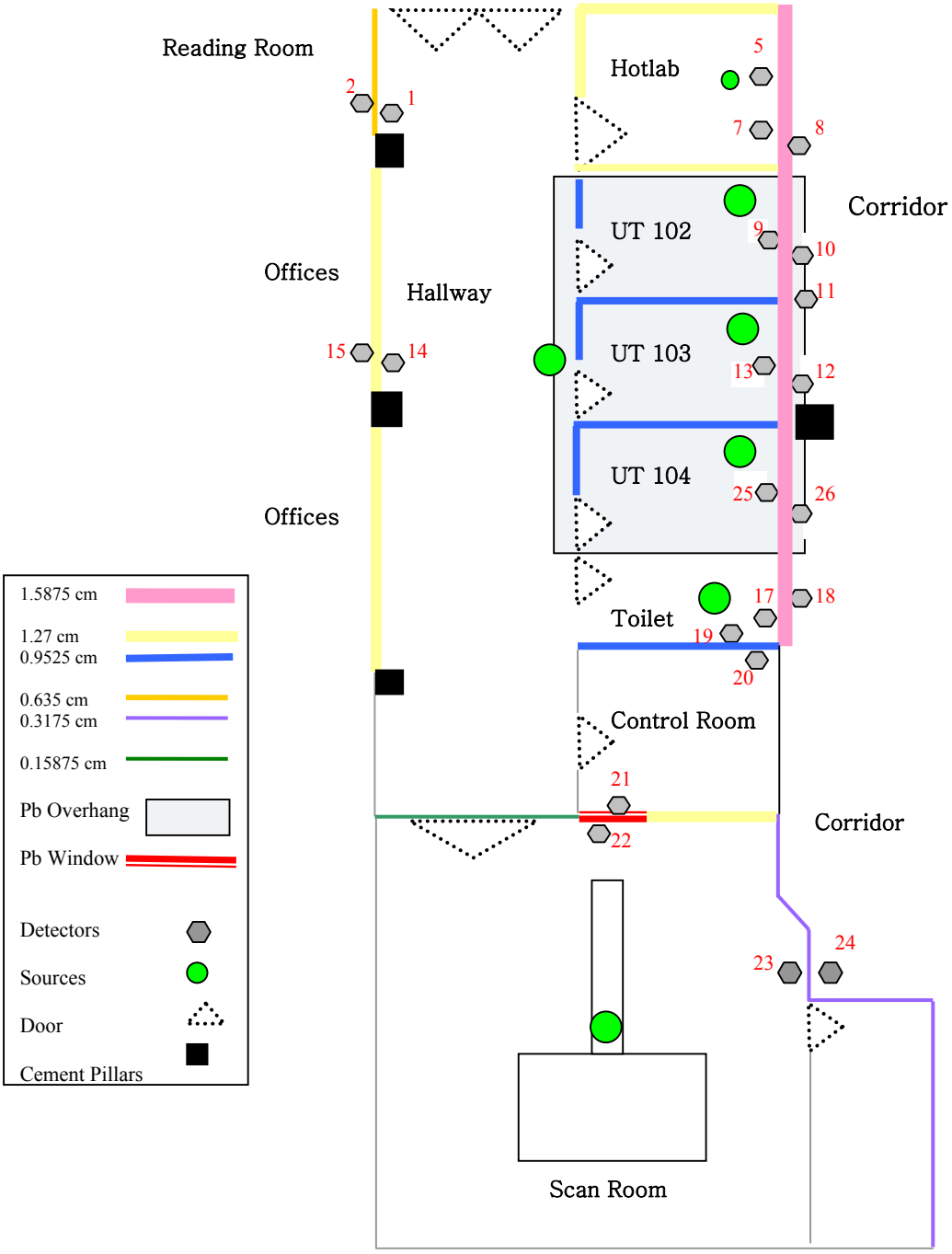

Fig. 9: The location of sources and detectors within the PET/CT suite (detectors 3, 4, & 6, not used)

The previous discussion focused primarily on the doses from PET. In reality, there is not only dose from PET, but also from the CT portion of the PET/CT unit, which

consists of low-energy x rays in the range of 40-150 kVp compared to the 511-keV photons for which the walls were designed. As a result, penetration of low-energy x rays through the relatively thick leaded-walls of the PET/CT suite is not significant. To separate the dose to the detectors inside the scanroom from PET, the dose from the CT portion of the exams was subtracted from the final dosimeter readings by running the CT portion of a "test" exam using a water phantom in place of the patient. An ionization chamber was placed in the scanroom to measure the integrated dose for the equivalent of one patient. This was done in two places within the scanroom: at the locations of detector 22 and detector 23.

Computational Methods

The computational methods used were based on the AAPM Task Group 108 report (Madsen et al 2006). Foremost, it should be noted that there were major simplifications made in preparation for the calculations. Both the detectors and sources (patients) were assumed to be points at approximately the same coordinates in space as the physical detectors and actual patients located in the PET/CT suite during the eight-week measurement period. In addition to the sources being considered as points, the sources were assumed to be static sources rather than the true life situation in which the sources were dynamic—walking from room to room within the suite. The mean free path of 511-keV photons in air is around 100 meters (Attix 2004) and so attenuation of the 511-keV photons through air around the suite was considered to be negligible. Another major assumption was that there was no attenuation attributed to the materials surrounding the lead in the walls (gypsum wallboard, supporting braces etc.), or objects

in the room (chairs, sinks, cabinets, etc.). The only structures modeled were the leaded walls.

The final summed doses were the result of several calculations, which were combined. Part I included assigning five "stages", or locations, for each patient: the uptake room (three uptake rooms total), hallway, toilet, scanroom, and back to the uptake room for dressing and checkout. Each of these stages accounted not only for the room where the patient was located, but for a set, finite period of time the patient was in that area. Fig. 10 depicts these five stages.

Fig. 10 illustrates the complexity of modeling patient movement in the PET/CT suite. Although the assumptions of source position in the uptake rooms, toilet, scanroom and hotlab seem to be fairly accurate, the position of the source in the hall is simply an estimate of where the majority of patient movement in the hallway occurred.

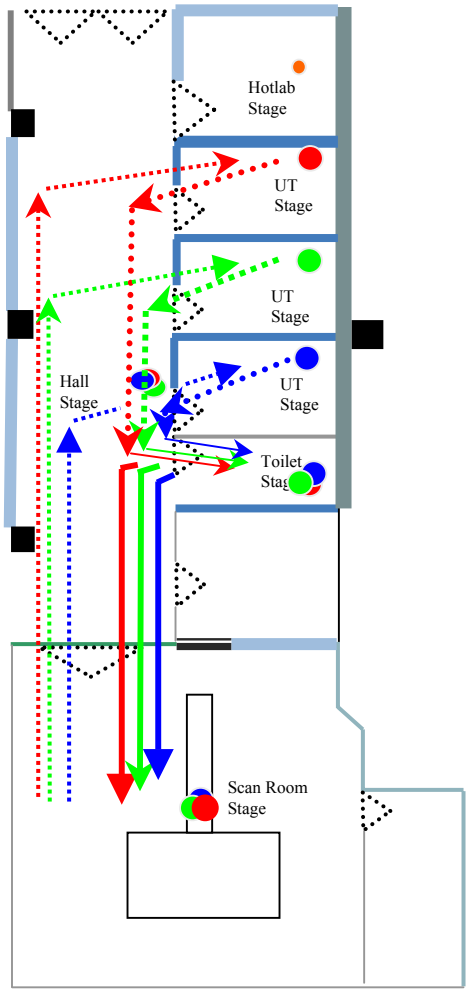

Fig. 10: The stages and rotation of a patient in each of the three uptake rooms

Using the decay constant of $^{18}\mathrm{F}$, λ, and the time, *t*, that the source was in a stage, the equivalent time, t_{eqv}, which accounts for radioactive decay was found as shown in Equation 3:

$$t_{eqv} = \int_{t_1}^{t_2} e^{-\lambda t} dt \,. \tag{3}$$

The variables t_1 and t_2 are the start and finish time of each stage.

Table 1 gives an overview of the time the sources were estimated to be in each stage along with the effective time calculated.

Table 1. Time assumptions of the sources at each stage.

Source Room	Total Time (min)	Time 1 t1 (min)	Time 2 t2 (min)	Equivalent Time Residence (min)
Hotlab	1	0	1	1.00
UT (Uptake)	59	1	60	49.0
Hallway	2	60	62	1.36
Toilet	5	62	67	3.33
Scanroom	30	67	97	17.9
UT (End)	10	97	107	5.25

The amount of radiation released from the source at each stage is shown in Equation 4:

$$R_{S,i} = t_{eqv} A\Gamma(1 - F_B) \tag{4}$$

where $R_{S,i}$ is the radiation released from one source (patient) during one stage; A is the activity of the administered dose, Γ is the specific gamma-ray constant and F_B is the factor that accounts for attenuation within the patient. AAPM recommended this factor to be 0.36 (Madsen et al 2006).

Part II of the calculations consisted of finding the distance between each detector and the possible eight sources listed in Table 1 (including three uptake rooms), as well as which leaded walls stood in-between each source-detector combination. Rarely would

particles travel orthogonally through the leaded wall on their way to the detector as shown in Fig. 11, so Equation 5 was used to calculate the actual through-distance, *d*, traveled for each horizontal wall (see Fig. 11):

$$d = \frac{D * h}{Y} \tag{5}$$

in this equation, *D* is the total distance from the source to the detector, *h* is the actual thickness of the lead slab and *Y* is the total distance in the y direction. Equation 5 was also used for vertical walls but altered slightly to account for the wall position.

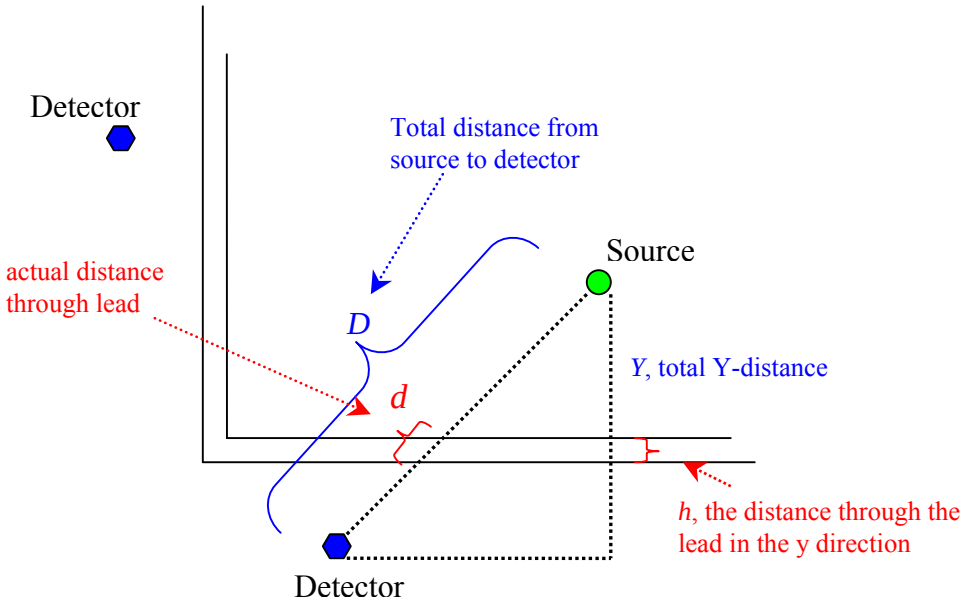

Fig. 11: Illustration of source to detector geometry

Attenuation of radiation is based in part, on the thickness of the attenuating material—in this case, lead. Therefore, once the actual distance through the lead wall

was determined, the transmission factor, or probability of radiation getting through the wall, could to be determined.

The simple calculations used empirical transmission data from AAPM Task Group 108 (Madsen et al 2006) in which the geometry of the beam intersection with the lead wall was orthogonal. In this case, the effective thickness was actually greater than the wall thickness because the angle of penetration was seldom 90°. This increased the effective thickness and provided significant increased absorption. However, there was some concern whether empirical orthogonal transmission data would still be valid considering the non-orthogonal geometry of this experiment. Modeling this scenario using MCNPX demonstrated that differences arising from these two situations were negligible and could not be used to explain potential sources of error. Fig. 12a illustrates how empirical data was collected based on orthogonal interception. Fig. 12b illustrates the actual scenario in which the angle of penetration was not 90°.

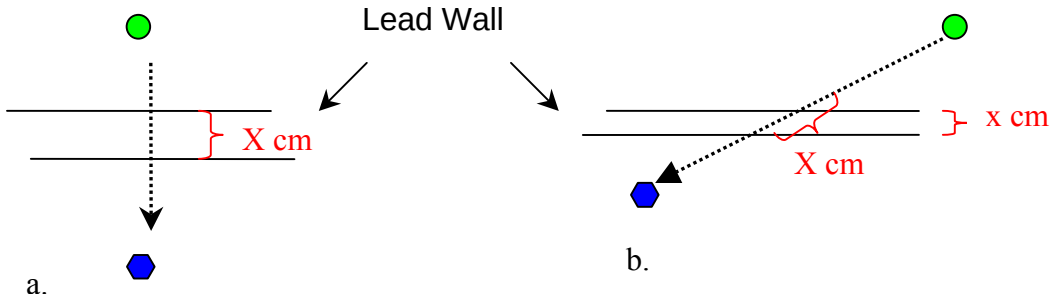

Fig. 12: a. Effective thickness of lead slab; b. Same effective thickness with different actual thickness

The AAPM Task Group report presents transmission data for 511-keV photons. These data points were plotted and fit with an exponential curve. Detailed results of the curve fit can be found in Appendix B. An equation was obtained from this curve fit and used to predict the transmission factor for radiation traveling through the various lead thicknesses. Combining transmission factors for each wall, by simple multiplication, resulted in a final factor that accounted for the attenuation of all walls through which the radiation would pass.

With Parts I and II complete, the amount of radiation released in each stage and the total transmission of radiation from each source to each detector was determined. Finding the dose for radiation going from source to detector required a simple distance correction and multiplication of the solutions from Parts I and II. This is shown in Equation 6:

$$\mathrm{K}_{d,S,i} = \frac{R_{S,i} * T_{d,S,i}}{D_{d,S,i}^{\,2}} \tag{6}$$

where $\mathrm{K}_{d,S,i}$ is the dose to an individual detector (d) for one stage (i) for one patient (S), $R_{i,S}$ is the released radiation for one stage and patient, $T_{d,S,i}$ is the total transmission, and $D_{d,S,i}$ is the total distance between the source and detector .

Individual detector doses for all five stages are brought together and a total dose, $K_{d,S}$ to each detector (d), for one patient (S), was calculated as shown in Equation 7:

$$K_{d,S} = \sum_{S} \frac{R_{S,i} T_{d,S,i}}{D_{d,S,i}^{2}} . \tag{7}$$

Once the average number of patients in each uptake room was taken into account, the total dose to each detector from one patient was found. Combining the doses from the total number of PET/CT patients in all three uptake rooms for the eight-week period left a final dose to be compared with the results of the physical measurements and the results from the MCNPX code. This is shown in Equation 8:

$$\mathrm{K}_d = \sum_{i=1}^{4} P_i \sum_{S=1}^{6} K_{d,S} \tag{8}$$

where K_d is the total dose to each detector and P_i is the number of patients in each stage. Dose from CT was not calculated.

The MCNPX Code

To ensure the techniques used to simulate the PET/CT suite at Scott & White Hospital were correct, the code MCNPX was used to simulate the transmission of 511-keV photons through lead. These results were compared to results contained in the AAPM Task Group 108 Report. Fig. 13 shows a slice of the geometry used in the MCNPX simulation.

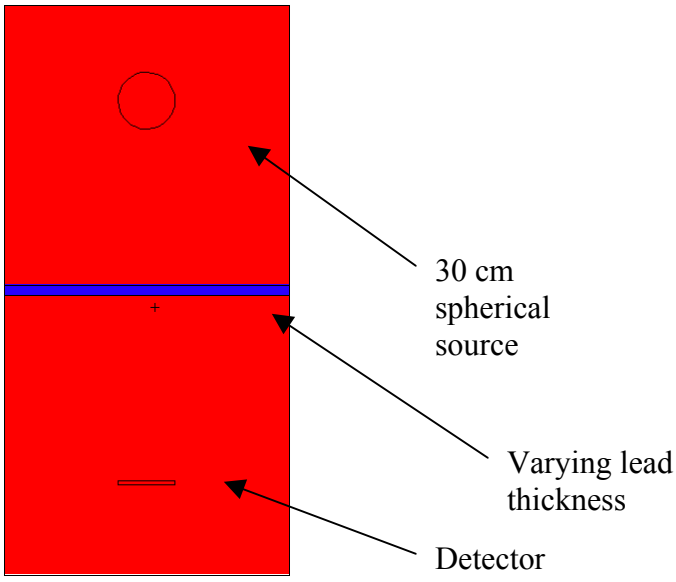

Fig. 13: MCNPX geometry

The results of the comparison are shown in Fig. 14. The closeness of the fluence estimates in the two simulations illustrate that the techniques used in the MCNPX simulation of the PET/CT suite were correctly implemented.

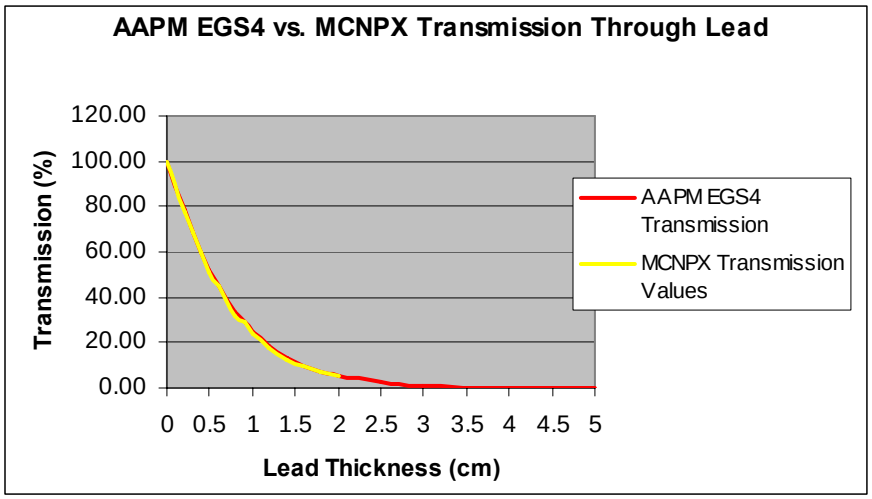

Fig. 14: AAPM EGS4 versus MCNPX transmission results

The MCNPX code for the PET/CT portion of the experiment was compiled using the more simplistic aspects of the computer program. As with the AAPM calculations, there were assumptions made in the MCNPX code. Most importantly, only the leaded walls and ceiling overhang of the suite were modeled, along with the cement ceiling, floor and 4 cement pillars in close proximity of the suite. Dry wall, supporting structures within the wall, and any steel in the ceiling were not modeled. If a wall was not leaded, it was not included in the code. The patient in the program was modeled as a constant 511-keV photon-emitting source. Each source was a 30 cm diameter sphere of water (ICRP 1959). As with the AAPM calculations, they were modeled static. The detectors were modeled as 30 cm diameter cylinders of air with a thickness of two centimeters, and with the center coordinates of each detector matching the coordinates in the empirical calculations. The large detector size provided a large detection area. In addition, output of the MCNPX code was in units of MeV g^{-1} which allowed the output to be compared to the measurements taken with the considerably smaller dosimeters.

Another key assumption made in the MCNPX code was that there was no attenuation from the PET/CT gantry itself. Although there is most probably attenuation in the gantry, detailed information on the gantry was proprietary and not readily available to individuals outside of Siemens.

Similar to the AAPM calculations, the code was divided into seven different source points: uptake 102, uptake 103, uptake 104, hall, toilet, scanroom and hotlab. A slice from the PET/CT suite modeled in MCNPX is shown in Fig. 15. The rectangle surrounding the suite is the area past which particles are no longer tracked.

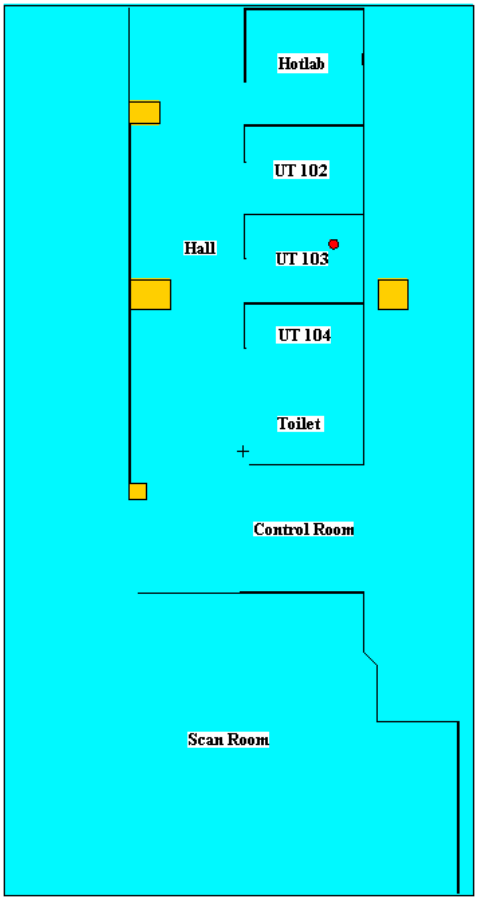

Fig. 15: MCNPX model plot

In each execution of the MCNPX code, there were some detectors too far and too many lead wall thicknesses away to receive significant doses from the source. In most instances, these detectors did not pass the statistical tests and so the results could not be considered reliable. These detectors were assumed to be zero and neglected for that particular source, although for closer sources they received significant and quantifiable doses that contributed to the final dose estimations.

The code simulation for each source was executed several times with a varying number of histories (100,000 – 2,000,000,000) in an effort for the greatest number of detectors to pass the statistical tests. Results passing all ten statistical tests were gathered from the various simulations and used in the final dose estimation.

Energy deposition tallies (detectors) were used in the MCNPX code. The results were presented in units of MeV g^{-1}. Converting the energy deposition to absorbed dose was necessary to compare the final MCNPX results with the AAPM calculations and physical measurements. The first step in the conversion process was to find the number of photons in each particular stage using computational methods. This was performed by using the activity of the administered patient dose, the effective time of the stage, which accounted for decay of the source at each stage, and the photon yield as shown in Equation 9:

$$\gamma_R = At_{eff}Y \tag{9}$$

where γ_R is the number of photons, A is the administered dose, t_{eff} is the effective time and Y is the photon yield. The photon yield is the total number of photons released in response to annihilation after each disintegration, which was found to be 1.96 (Lide 1994).

Monte Carlo codes allow the user to simulate a situation using only a fraction of the radiation that may exist in the real-life situation. This number of histories executed is specified by the user, and used in this case, by the code to estimate the average energy deposition in each detector. The ratio, *T*, between the number of photons in the real situation, γ_R, to the number of particles/photon histories simulated in the code, γ_{MC}, can be calculated as shown in Equation 10, and used to interpret the results from the MC code:

$$T = \frac{\gamma_R}{\gamma_{MC}}. \tag{10}$$

Quantifiable dose, K_{MC}, can be found from the relationship between the ratio of photons, *T*, and energy deposition, *S*, as shown in Equation 11:

$$K_{MC} = ST. \tag{11}$$

As in the AAPM calculations, the dose calculated in Equation 6 is simply the dose to the detector for one stage of one patient. To obtain accurate results, doses to each detector from every stage of each patient were combined as shown in Equation 7 of the AAPM calculations. Once again, this was done for every detector and then multiplied by the number of patients. As in the AAPM calculations, radiation from CT was not accounted for within the code. Input to the code in this experiment and a sample result can be seen in Appendix A.

CHAPTER IV

RESULTS AND DISCUSSION

Table 2 shows the results from the physical measurements as well as computational and MCNPX calculations. Results denoted "CT corrected" were dosimeters inside the scanroom that had the added component of CT. An estimated dose per patient from CT was subtracted from the final measurement. The result denoted "Possible error in measurement" fell from the wall sometime during the eight week measurement period. Dosimeters that did not pass all ten statistical tests are labeled "Incomplete results."

Comparing the AAPM calculations with the dosimeter measurements, one can see that the results are, for the most part, comparable. The contribution of each source to individual dosimeter results can be found in Appendix C. There are a few locations for which there are significant differences. Two of those locations include detectors five and seven that were located in the hotlab. Assumptions were made about the hotlab, mainly as a result of inconsistencies with the daily routine in the hotlab itself. Detector 5 was located directly in front of the dose calibration unit, where every patient dose of ^{18}F was calibrated before patient injection. It is possible that the one minute time estimation of the AAPM calculations for each unshielded dose calibration was more than the actual time it took for the calibration. This may account for the higher detector reading. The dose accumulated by Detector 7 in the suite was actually lower than the AAPM calculations and once again may be a result of assumptions. This detector was located in front of the 'pigs' (lead containers) in which the daily doses were held. While patient doses inside the pigs are heavily shielded and neglected in the calculations, it is possible

that more radiation than expected escaped accounting for a higher measurement than expected. It is also very possible that attenuating material was in-between Detector 7 the unshielded patient doses being calibrated; very possibly the shielding of the calibration unit itself. This is in contrast to the AAPM calculations, where it was assumed that nothing was between the calibrating doses and the detector accounting for a higher dose

Table 2. Final detector results.

	AAPM	MCNPX	Physical	
Detector	(mrem)	(mrem)	(mrem)	
1	14	1*	1	
2	1	2*	2	
5	248	9*	46	
7	44	1961	58	
8	2	14	2	
9	418	427	81	
10	13	25	2	
11	6	6	1	
12	21	17	33	
13	406	435	107	
14	63	18	11	
15	3	4	5	
17	116	1189*	66	
18	8	51	1	
19	121	42*	104	
20	30	199	35	
21	21	74	29	
22	26	21*	0	▫
23	28	97	52	▫
24	18	1*	2	◊
25	524	680*	182	
26	30	27	3	

* Incomplete results (did not pass all statistical tests)
◊ Possible error in measurement due to movement of detector
▫ CT corrected

Comparing the AAPM calculations with the dosimeter measurements, one can see that the results are, for the most part, comparable. The contribution of each source to individual dosimeter results can be found in Appendix C. There are a few locations for which there are significant differences. Two of those locations include detectors five and seven that were located in the hotlab. Assumptions were made about the hotlab, mainly as a result of inconsistencies with the daily routine in the hotlab itself. Detector 5 was located directly in front of the dose calibration unit, where every patient dose of ^{18}F was calibrated before patient injection. It is possible that the one minute time estimation of the AAPM calculations for each unshielded dose calibration was more than the actual time it took for the calibration. This may account for the higher detector reading. The dose accumulated by Detector 7 in the suite was actually lower than the AAPM calculations and once again may be a result of assumptions. This detector was located in front of the 'pigs' (lead containers) in which the daily doses were held. While patient doses inside the pigs are heavily shielded and neglected in the calculations, it is possible that more radiation than expected escaped accounting for a higher measurement than expected. It is also very possible that attenuating material was in-between Detector 7 the unshielded patient doses being calibrated; very possibly the shielding of the calibration unit itself. This is in contrast to the AAPM calculations, where it was assumed that nothing was between the calibrating doses and the detector accounting for a higher dose calculation.

There were several other detectors in the AAPM calculations with values lower than the actual measurements. None of these differences was significant except for detectors 7 and 12. There is a possibility that no lead was actually placed behind the

cement pillars between uptake rooms 103 and 104. If no lead is there, this would explain a higher dose in this area that was not accounted for in the shielding design or AAPM calculations.

Detectors 9, 13 and 25 had results in both the AAPM calculations and MCNPX estimations that were much higher than the actual measurements. There are several explanations, ranging from unaccounted attenuating materials in the room to the fact that a point source was used in the hand calculations and a simple volume source was used in the MCNPX simulation rather than the actual complex volume source of the patient.

The main point to be made regarding the AAPM calculations is that although several were much higher than the measured doses, most of the calculations erred on the conservative side, which is the desired effect when designing radiation shielding.

The MCNPX results, however, showed no real consistency when compared to the measurements: some were much higher than the measurements and some compared well with the AAPM calculations. However, other MC results were not able to converge to a statistically significant value. Examination of the MCNPX estimated doses in the PET/CT suite demonstrated inconsistency in the results. Based on the vastness of the program itself, differences between the MCNPX estimates and the measurements are somewhat hard to reconcile, but some speculations can be made.

There were eight detectors (annotated by * in Table 2) receiving significant doses from sources near, or in the same room as they were located; that would not converge with statistically relevant values. The program was executed with several different numbers of histories, both large and small. In addition, a variance reduction technique

was used, which focused directly on each of these 'problem' detectors. In the end, these techniques resulted in statistically relevant values for only a few cases.

On the other hand, Detectors 7 and 17 had estimated doses so high that they were unrealistic in comparison to the measured doses. Although no explanation is available for these results, it suggests potential problems in using MCNPX for such a complex problem.

There were several detectors in the Monte Carlo simulation that gave results between the physical measurements and the AAPM calculations; this was the original hypothesis, though only a few detectors in the simulation showed such results. Once again, overall inconsistency in the Monte Carlo results leave these few valid cases questionable.

The methods and results used in the design of the MCNPX code were discussed with a MCNPX consultant, Bill Hamilton. He agreed that the results were less than desirable. Given that the common techniques used in this program produced unreliable results, convergence to statistically significant values may not be a task fit for such a complex problem.*

Although it appears that the MCNPX code is not suitable to model a PET/CT suite, there are aspects of the code that could be useful. One such aspect is the mesh tally, which graphically displays energy deposition per unit volume. The mesh tally allows the user to "see" places within the model where the energy deposition may be highest or lowest; in other words, places of interest. For radiation safety, "hot spots" may need special consideration in shielding design. An example of the results of a mesh tally with the source in uptake room 102 can be seen in Fig. 16. It can be seen that the

energy deposition is highest in room 102. Points further away from the source, such as the scanroom, show less energy deposition. The mesh tally plot does not provide detail, but more of an overview of the radiation transport in the experiment. In Fig. 16, areas of the highest energy deposition are shaded red, while areas of lowest energy deposition are shaded blue.

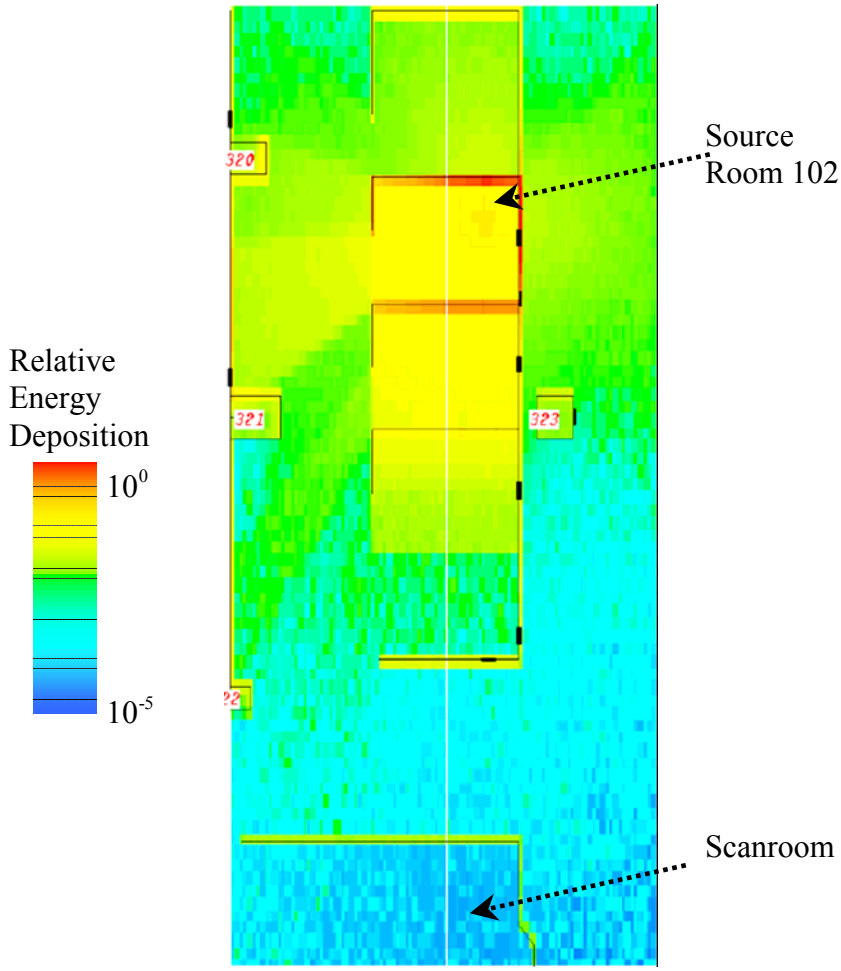

Fig. 16: MCNPX mesh-tally plot of energy deposition

---

* **Hamilton** B. Personal Communication, HQC Services; 2006.

As in most computational approaches to dosimetry, a number of simplifying assumptions were made. These assumptions can also be sources of error when comparing with measurements. One possible source of error was in the positioning of each detector. Each detector was placed flat on the wall with the front of the detector facing the known sources. However, radiation can impinge on the detector from various angles. To test the angular dependence of the Landauer badges, a short experiment was conducted. Landauer Al_2O_3:C detectors were placed at a constant distance from a ^{18}F source, but at different angles. The results from this exposure are in Table 3 with more detailed results in Appendix D.

Table 3. Angular dependence of the OSL.

Degrees	**Average Measurement** (mrem)
0	71 ± 0.40
30	71 ± 2.19
45	74 ± 2.61
60	103 ± 0.48
90	50 ± 1.92

At the point of greatest difference (60°), there was a 32% over-response between the measurement at 0° and 60°, with 90° trailing close behind with a 30% under-response. These are discrepancies that suggest up to an approximate 30% error in the amount of radiation the detectors were actually able to detect.

CHAPTER V

CONCLUSIONS

Computational methods and dose estimates obtained using MCNPX were compared with measurements made with dosimeters placed around the PET/CT suite for a measurement period of eight weeks. These results provided useful insights on the most accurate and reliable methods in designing shielding for a PET/CT suite. Although the traditional dose calculation method results in values higher than actual readings, it errs on the conservative side, which is the desired outcome for radiation safety. MCNPX estimations on the other hand, had a few results that appeared to be reliable; however, the results were not consistent and, in several cases, the calculations were not able to acquire statistically-significant results. Although there are aspects of MCNPX that could be of a help in designing a PET/CT suite, such as the mesh tally (which could assist in locating "hot spots"), it is beyond the scope of the typical "once-in-a-while" user to both model a suite and ensure the radiation safety of patients and workers using these results. Therefore, it has been concluded that the traditional methods of dose calculations are still the most reliable and efficient route to proper PET/CT shielding.

REFERENCES

Alazraki N, Mishkin FS (Ed.). Fundamentals of nuclear medicine. New York: The Society of Nuclear Medicine; 1991.

Attix F. Introduction to radiological physics and radiation dosimetry. Weinheim: WILEY-VCH Verlag GmbH & Co. KGaA; 2004.

Bushong SC. Radiologic science for technologists. St. Louis: Mosby, Inc.; 2001.

Cho Z, Jones J, Singh M. Foundations of medical imaging. New York: John Wiley & Sons, Inc.; 1993.

Frame PW. A history of radiation detection instrumentation. Health Phys. 87(2):111-135; 2004.

Hendee WR, ER Ritenour. Medical imaging physics 4th edition. New York: Wiley-Liss, Inc.; 2002.

Hendricks J. A Monte Carlo code for particle transport. Los Alamos Science 22: 30-43; 1994.

Hendricks J and Culbertson CN. An assessment of MCNP weight windows. LA-UR-00-55; May 2000.

International Commission on Radiological Protection. Report of committee II on permissible dose for internal radiation. Oxford: Pergamon Press; 1959.

Landauer. OSL Dosimetry. Available at: www.landauerinc.com. Accessed 2 July 2006.

Lide D. Handbook of chemistry and physics 1913-1995. Boca Raton, FL: CRC Press; 1994.

Madsen MT, Anderson JA, Halama JR, Kleck J, Simpkin DJ, et al. AAPM Task Group 108: PET and PET/CT shielding requirements. Med Phys 33: 4-15; 2006.

Metropolis N. The beginning of the Monte Carlo method. Los Alamos Science Special Issue: 125-130; 1987.

National Council on Radiation Protection (NCRP). Evaluation of the linear-nonthreshold dose-response model for ionizing radiation, NCRP Report No. 136; 2001.

National Nuclear Data Center. Nuclear Decay Data in the MIRD Format. Available at: http://www.nndc.bnl.gov/mird/. Accessed 1 August 2006.

Pelowitz D (Ed.). MCNPX user's manual version 2.5.0, Los Alamos, NM: Los Alamos National Laboratory Report; LA-CP-05-0369; 2005.

Radiology. Nuclear medicine PET basics. Available at: http://www.radiology-info.org/nuclear-medicine-positron-emission-tomography.html. Accessed 1 August 2006.

Siemens. Nuclear medicine products and solutions. Available at: http://www.medical.siemens.com/webapp/wcs/stores/servlet/ProductDisplay?productId=143899&storeId=10001&langId=-11&catalogId=-11&catTree=100001,12788,12756*2613447887&level=0. Accessed 1 August 2006.

U.S. Nuclear Regulatory Commission. Title 10 code of federal regulations part 20—standards for protection against radiation. Washington, DC: US Government Printing Office; 1992.

Supplemental Sources Consulted

Blizard E (Ed.). Reactor handbook volume III part B shielding. New York: John Wiley & Sons, Inc.; 1962.

Bushberg JT, Seibert JA, Leidholdt EM, Boone JM. The essential physics of medical imaging. Baltimore: Williams & Wilkins; 1994.

Knoll G. Radiation detection and measurement. Hoboken, NJ: John Wiley & Sons, Inc.; 2000.

Schultis JK, Faw RE. MCNP programming basics. Available at: ww2.mne.ksu.edu/~jks/MCNPprmr.pdf. Accessed 10 August 2006.

Turner J. Atoms, radiation, and radiation protection. New York: John Wiley & Sons; 1995.

APPENDIX A

Input code for source in uptake room 104

```
PET CT Suite Model
C datapath=C:\mcnpx\data
C
C _____________________________________________________________________________
C Cell Cards                                                                   |
C _____________________________________________________________________________
c Cell#  Mat#  Density      Geom       Imp
  31      1    -11.34       -1         imp:p=1           $ wall C
  32      1    -11.34       -2         imp:p=1           $ wall A
  33      1    -11.34       -3         imp:p=1           $ wall B
  34      1    -11.34       -4         imp:p=1           $ wall D
  35      1    -11.34       -5         imp:p=1           $ wall E
  36      1    -11.34       -6         imp:p=1           $ wall F
  37      1    -11.34       -7         imp:p=1           $ wall G
  38      1    -11.34       -8         imp:p=1           $ wall H
  39      1    -11.34       -9         imp:p=1           $ wall I
  310     1    -11.34       -10        imp:p=1           $ wall J
  311     1    -11.34       -11        imp:p=1           $ wall K1
  3110    1    -11.34       -110       imp:p=1           $ wall K2
  312     1    -11.34       -14        imp:p=1           $ wall M
  313     1    -11.34       -12        imp:p=1           $ wall O
  314     1    -11.34       -13        imp:p=1           $ wall N
  315     1    -11.34       -16        imp:p=1           $ wall L1
  3151    1    -11.34      (17 -171 -172 173 174 -175) imp:p=1 $wall L2
  3152    1    -11.34       -18        imp:p=1           $wall L3
  3153    1    -11.34       -19        imp:p=1           $wall L4
  3154    1    -11.34       -20        imp:p=1           $wall L5
C Cell below (316) is the air outside of the walls
  316     2    -0.00120484 (1 2 3 4 5 6 7 8 9 10 11 12 13 14 15 16 18 19 20 &
        22 23 24 25 26 27 110 -21 200 201 202 205 207 208 209 210 211 212 &
        213 214 215 217 218 219 220 221 222 223 224 225 226 227 501 &
        #(17 -171 -172 173 174 -175)) imp:p=1
C
  317     0                 21        imp:p=0  $world outside surf 21(sphere)
  318     1    -11.34       -200       imp:p=1  $ceiling overhang
  319     3    -4.8         -15        imp:p=1  $leaded window
  320     4    -2.85        -22        imp:p=1  $column X
  321     4    -2.85        -23        imp:p=1  $column Y
  322     4    -2.85        -24        imp:p=1  $column Z
  323     4    -2.85        -25        imp:p=1  $column W
  326     4    -2.85        -26        imp:p=1  $cement flr
  327     4    -2.85        -27        imp:p=1  $cement ceiling
C ------------------------------------------------------------
C Detector Cells
C ------------------------------------------------------------
  401     2    -0.00120484  -201         imp:p=1  $detector 1
  402     2    -0.00120484  -202         imp:p=1  $detector 2
  405     2    -0.00120484  -205         imp:p=1  $detector 5
  407     2    -0.00120484  -207         imp:p=1  $detector 7
  408     2    -0.00120484  -208         imp:p=1  $detector 8
  409     2    -0.00120484  -209         imp:p=1  $detector 9
  410     2    -0.00120484  -210         imp:p=1  $detector 10
  411     2    -0.00120484  -211         imp:p=1  $detector 11
  412     2    -0.00120484  -212         imp:p=1  $detector 12
  413     2    -0.00120484  -213         imp:p=1  $detector 13
  414     2    -0.00120484  -214         imp:p=1  $detector 14
  415     2    -0.00120484  -215         imp:p=1  $detector 15
  417     2    -0.00120484  -217         imp:p=1  $detector 17
  418     2    -0.00120484  -218         imp:p=1  $detector 18
  419     2    -0.00120484  -219         imp:p=1  $detector 19
  420     2    -0.00120484  -220         imp:p=1  $detector 20
  421     2    -0.00120484  -221         imp:p=1  $detector 21
  422     2    -0.00120484  -222         imp:p=1  $detector 22
  423     2    -0.00120484  -223         imp:p=1  $detector 23
  424     2    -0.00120484  -224         imp:p=1  $detector 24
```

```
  425     2    -0.00120484  -225         imp:p=1  $detector 25
  426     2    -0.00120484  -226         imp:p=1  $detector 26
  427     2    -0.00120484  -227         imp:p=1  $detector 27
C ------------------------------------------------------------
C Source Cells
C ------------------------------------------------------------
C    601   5     -1.00        -501         imp:p=1  $Uptake Rm 102 *************
C    601   5     -1.00        -501         imp:p=1  $Uptake Rm 103 *************
 601   5     -1.00        -501         imp:p=1  $Uptake Rm 104 *************!!!!
C    601   5     -1.00        -501         imp:p=1  $Toilet ********************
C    601   5     -1.00        -501         imp:p=1  $Hall   ********************
C    601   5     -1.00        -501         imp:p=1  $Scanroom ******************
C    601   5     -1.00        -501         imp:p=1  $Hotlab ********************

C ____________________________________________________________________________
C Surface Cards (width of lead only! Does not include drywall or Gantry)
C ____________________________________________________________________________
C
C Surf# Name  xmin   xmax     ymin      ymax    zmin    zmax
  1     RPP   590.4  592.0   -440.6499 739.2    0       213.4  $wall C
  2     RPP   283.2  592.0    739.2002 740.5    0       213.4  $wall A
  3     RPP   283.2  284.47   552.0    739.2    0       213.4  $wall B
  4     RPP   283.2  590.4    436.8    438.1    0       213.4  $wall D
  5     RPP   283.2  284.15   340.8    436.799  0       213.4  $wall E
  6     RPP   283.2  590.399  206.4    207.35   0       213.4  $wall F
  7     RPP   283.2  284.15   91.20    206.399  0       213.4  $wall G
  8     RPP   283.2  590.399 -24.00   -23.05    0       213.4  $wall H
  9     RPP   283.2  284.15  -139.2   -24.001   0       213.4  $wall I
  10    RPP   297.6  592.0   -441.6   -440.65   0       213.4  $wall J
  11    RPP   369.6  590.4   -772.8   -771.53   0       213.4  $wall K1
  110   RPP   273.6  369.6   -772.8   -771.53   0       96.5   $wall K2
  12    RPP  -14.40 -14.336   499.2    740.5    0       213.4  $wall O
  13    RPP  -14.40 -13.76   -489.6    441.6    0       213.4  $wall N
  14    RPP   9.6    273.599 -772.8   -772.6412 0       213.4  $wall M
  15    RPP   273.6  369.599 -772.8   -771.53   96.501  209.6  $PB Win P
  16    RPP   590.4  590.7   -926.399 -771.53   0       213.4  $wall L1
  18    RPP   624.0  624.32  -1108.0  -960.001  0       213.4  $wall L3
  19    RPP   624.0  835.19  -1108.3  -1108.001 0       213.4  $wall L4
  20    RPP   835.2  835.52  -1564.8  -1108.0   0       213.4  $wall L5
  22    RPP  -14.40  62.4     441.601  499.199  0       213.4  $column X
  23    RPP  -13.759 91.2    -38.4     38.4     0       213.4  $column Y
  24    RPP  -14.40  28.8    -532.8   -489.601  0       213.4  $column Z
  25    RPP   628.8  705.6   -38.4     38.4     0       213.4  $column W
  26    RPP  -336.0  873.6   -1555.2   748.8   -12.0007 -0.0001 $Cement Flr
  27    RPP  -336.0  873.6   -1555.2   748.8    439.84  450.00 $Cement Ceiling
  200   RPP   283.4  592.0   -249.6    438.1    429.045 429.68 $Pb overhang (ceiling)
  21    RPP  -337.0  875.0   -1570.0   749     -13      454.0  $New Outside World
  17    P     1 1 0 -335.999                             $L2
  171   P     1 1 0 -335.6825                            $L2
  172   PY   -926.4                                      $pln connects L1 & L2
  173   PY   -960.0                                      $pln connects L2 & L3
  174   PZ    0                                          $plane at FLR L2
  175   PZ    213.4                                      $plane at ceiling  L2
C ------------------------------------------------------------------
C Detector Surfuces
C ------------------------------------------------------------------
C Surf# Name  V(x)     V(y)    V(z)    h(x)     h(y)    h(z)  radius
  201   RCC -12.400   542.4   139.7    2        0       0     15      $detector 1
  202  RCC  -16.336   542.4   139.7   -2        0       0     15      $detector 2
  205  RCC   588.4    609.6   114.3   -2        0       0     15      $detector 5
  207  RCC   588.4    609.6   48.30   -2        0       0     15      $detector 7
  208  RCC   594.0    609.6   48.30    2        0       0     15      $detector 8
  209  RCC   588.4    326.4   144.8   -2        0       0     15      $detector 9
  210  RCC   594.0    326.4   144.8    2        0       0     15      $detector 10
  211  RCC   594.0    216.0   144.8    2        0       0     15      $detector 11
  212  RCC   594.0    96.0    144.8    2        0       0     15      $detector 12
  213  RCC   588.4    96.0    144.8   -2        0       0     15      $detector 13
  214  RCC  -12.400   72.0    139.7    2        0       0     15      $detector 14
  215  RCC  -15.76    72.0    139.7   -2        0       0     15      $detecotr 15
  217  RCC   588.4   -398.4   139.7   -2        0       0     15      $detector 17
  218  RCC   594.0   -398.4   139.7    2        0       0     15      $detector 18
```

```
  219  RCC   528.0   -438.65  139.7    0        2       0     15      $detector 19
  220  RCC   528.0   -443.60  139.7    0       -2       0     15      $detector 20
  221  RCC   321.6   -769.53  155.5    0        2       0     15      $detector 21
  222  RCC   321.6   -774.8   155.5    0       -2       0     15      $detector 22
  223  RCC   622.0   -1080.0  139.7   -2        0       0     15      $detector 23
  224  RCC   626.32  -1080.0  139.7    2        0       0     15      $detector 24
  225  RCC   588.4   -134.4   139.7   -2        0       0     15      $detector 25
  226  RCC   594.0   -134.4   139.7    2        0       0     15      $detector 26
  227  RCC   707.6    1.000   139.7    2        0       0     15      $detector 27
C ---------------------------------------------------------------------
C Source Surfaces
C ---------------------------------------------------------------------
C     501  S  514.4  360.8  105.48 -15             $Uptake Rm 102 ***************
C     501  S  514.4  130.4  105.48  15             $Uptake Rm 103 ***************
 501  S  514.4 -100.0  105.48  15             $Uptake Rm 104 ***********!!!!!!!!!
C     501  S  514.4 -364.65 105.48  15             $Toilet ***********************
C     501  S  207.2  106.2  105.48  15             $Hall   ***********************
C     501  S  321.6 -1185.6 81.28   15             $Scanroom *********************
C     501  S  207.2  106.2  105.48  2              $Hotlab ***********************

C _____________________________________________________________________________
C Data Cards
C _____________________________________________________________________________
C
C Material zaid     fraction
C
C Lead
  M1       82000.04p    1.0
C
C Air                              rho = 0.00120484 g/cc  (ICRU Report 49)
  M2       6000.04p    -0.000125
           7000.04p    -0.755267
           8000.04p    -0.231781
           18000.04p   -0.012827
C
C Leaded Window
  M3       82000.04p    0.106025
           16000.04p    0.666667
           14000.04p    0.227308
C
C Concrete/Cement                  rho = 2.85 g/cc
  M4       001001.04p   0.11698245
           001002.04p   0.00001755
           008016.04p   0.60796842
           008017.04p   0.000231579
           014028.04p   0.25344804
           014029.04p   0.01283316
           014030.04p   0.0085188
C
C Water                           rho = 1.00 g/cc
  M5       1001.04p     2.0
           8016.04p     1.0
C
  Mode p
  nps= 5000000
C imp:1
C
C Source  Energy(MeV) Position                    Radius
C ------------------------------------------------------------------------------
C    sdef    Erg=0.511   Pos=514.4 360.8 105.48     Rad=d1  $Uptake Rm 102 ***
C       SI1  0  15                                           $Rad  102 *****
C       SP1 -21 2                                            $part dist 102
C   sdef     Erg=0.511   Pos=514.4  130.4  105.48   Rad=d1  $Uptake Rm 103 ***
C       SI1  0  15                                           $Rad  103 *****
C       SP1 -21 2                                            $part dist 103
 sdef    Erg=0.511   Pos=514.4 -100.0  105.48   Rad=d1  $Uptake Rm 104 ***!!!!
   SI1  0  15                                             $Rad  104 *****!!!!!
   SP1 -21 2                                              $part dist 104 !!!!!
C    sdef    Erg=0.511   Pos=207.2  106.2  105.48   Rad=d1  $Hallway       ***
C      SI1  0  15                                           $Rad  Hall *****
C      SP1 -21 2                                            $part dist Hall
```

```
C    sdef    Erg=0.511   Pos=514.4 -364.65 105.48   Rad=d1  $Toilet        ***
C      SI1  0  15                                             $Rad  Toilet ***
C      SP1 -21 2                                              $part dist Toilet
C    sdef    Erg=0.511   Pos=321.6 -1185.6 81.28    Rad=d1  $ScanRm         **
C      SI1  0  15                                             $Rad  ScanRm ***
C      SP1 -21 2                                              $part dist ScanRm
C    sdef    Erg=0.511   Pos=207.2 106.2 105.48     Rad=d1  $Hotlab         **
C      SI1  0  2                                              $Rad  HotLab ***
C      SP1 -21 2                                              $part dist Hotlab
C
C Tallies
C ------------------------------------------------------------------------------
 WWG 126 0
 WWN1:p 0.5 53
 WWP:p  4j -1
 MESH geom=rec   ref=514.4 -100 105.48   origin=496.4 -442 -17
      imesh  531.4 595           iints  1 40
      jmesh -117  -82   -22      jints 10 1 1
      kmesh  90    122   456     kints 20 1 10
C
C  Pt.Det   Cell
C  ---------------------------------------------------------------------------
  F6:p      401                                $Detector 1
  F16:p     402                                $Detector 2
  F26:p     405                                $Detector 5
  F36:p     407                                $Detector 7
  F46:p     408                                $Detector 8
  F56:p     409                                $Detector 9
  F66:p     410                                $Detector 10
  F76:p     411                                $Detector 11
  F86:p     412                                $Detector 12
  F96:p     413                                $Detector 13
  F106:p    414                                $Detector 14
  F116:p    415                                $Detector 15
  F126:p    417                                $Detector 17
  F136:p    418                                $Detector 18
  F146:p    419                                $Detector 19
  F156:p    420                                $Detector 20
  F166:p    421                                $Detector 21
  F176:p    422                                $Detector 22
  F186:p    423                                $Detector 23
  F196:p    424                                $Detector 24
  F206:p    425                                $Detector 25
  F216:p    426                                $Detector 26
  F226:p    427                                $Detector 27
```

Sample output for source in uptake room 104

```
                      tally   36
       nps      mean      error  vov    slope fom
    256000   0.0000E+00  0.0000 0.0000  0.0  0.0E+00
    512000   0.0000E+00  0.0000 0.0000  0.0  0.0E+00
    768000   9.6948E-12  1.0000 1.0000  0.0  4.3E-01
   1024000   7.2711E-12  1.0000 1.0000  0.0  3.2E-01
   1280000   5.8169E-12  1.0000 1.0000  0.0  2.6E-01
   1536000   4.8474E-12  1.0000 1.0000  0.0  2.2E-01
   1792000   9.0732E-12  0.7096 0.5140  0.0  3.7E-01
   2048000   7.9391E-12  0.7096 0.5140  0.0  3.2E-01
   2304000   7.0570E-12  0.7096 0.5140  0.0  2.9E-01
   2560000   7.7484E-12  0.6090 0.4355  0.0  3.5E-01
   2816000   8.8627E-12  0.5257 0.3361  0.0  4.3E-01
   3000000   8.3192E-12  0.5257 0.3361  0.0  4.0E-01
```

APPENDIX B

Transmission Factors

The AAPM Task Group report presents transmission data for 511 keV photons. These data points were plotted and fit with an exponential curve shown below. An equation was obtained from this curve fit and used to predict the transmission factor for radiation traveling through the various lead thicknesses.

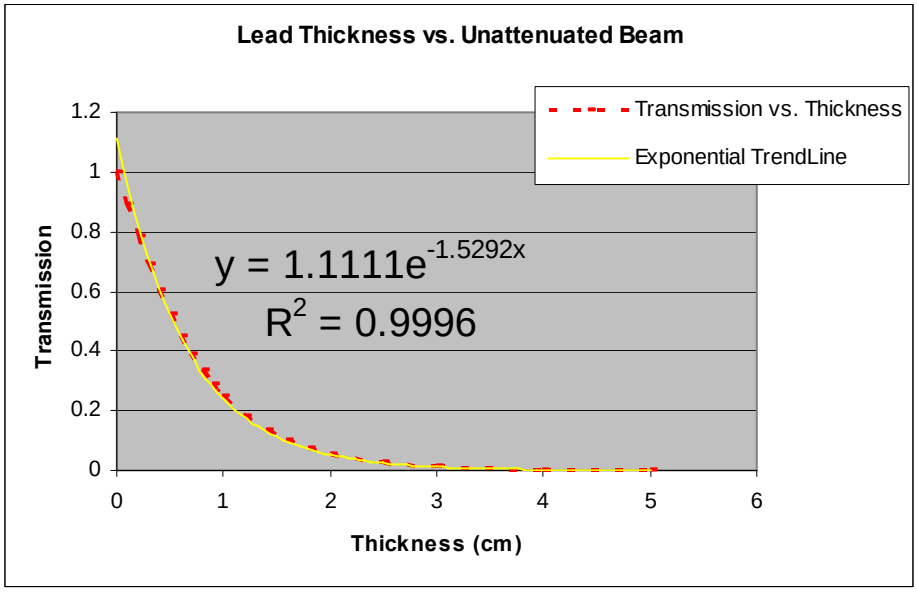

APPENDIX C

Source Contributions to Each Detector

AAPM Calculations

Source / Detector	UT102	UT103	UT104	Hallway	Toilet	Scan Rm	Hotlab	Total
	(Uptake + Uptake End)							
	mrem							
1	0.02	0.71	0.16	11.81	0.10	0.83	0.12	13.75
2	0.01	0.23	0.04	0.36	0.02	0.01	0.05	0.70
5	4.18	0.52	0.08	0.01	0.01	0.00	243.34	248.14
7	3.81	0.50	0.08	0.01	0.01	0.00	40.06	44.46
8	0.00	0.00	1.96	0.00	0.00	0.00	0.19	2.16
9	234.85	15.42	167.16	0.25	0.07	0.00	0.49	418.26
10	12.95	0.02	0.00	0.00	0.00	0.00	0.00	12.97
11	0.42	5.22	0.00	0.06	0.00	0.22	0.00	5.92
12	0.00	20.65	0.03	0.19	0.00	0.00	0.00	20.87
13	6.02	374.64	19.79	4.58	0.63	0.02	0.04	405.73
14	5.32	2.79	0.13	51.82	1.17	1.51	0.03	62.76
15	0.64	0.43	0.02	1.80	0.10	0.00	0.00	3.00
17	0.22	2.73	41.24	0.86	70.55	0.14	0.00	115.74
18	0.00	0.00	0.00	0.07	4.14	4.24	0.00	8.45
19	0.20	2.44	34.00	3.45	80.40	0.18	0.00	120.67
20	0.05	0.62	8.48	0.23	16.12	0.00	4.23	29.73
21	0.02	0.23	1.97	7.14	0.59	11.23	0.00	21.17
22	0.02	0.15	1.30	7.01	0.58	16.96	0.00	26.02
23	0.00	0.00	0.00	0.06	0.00	28.20	0.00	28.26
24	0.00	0.00	0.00	0.02	0.00	18.13	0.00	18.16
25	0.49	9.69	503.92	0.43	9.21	0.09	0.00	523.84
26	0.00	0.00	29.38	0.03	0.01	0.09	0.00	29.52

MC Estimations

Source / Detector	UT102	UT103	UT104	Hallway	Toilet	Scan Rm	Hotlab	Total
	(Uptake + Uptake End)							
	mrem							
1	1.08	0.00	0.03	0.00	0.20	0.05	0.00	1.37
2	0.96	0.00	0.05	0.61	0.26	0.14	0.00	2.02
5	7.50	0.40	0.08	0.37	0.23	0.00	0.00	8.59
7	6.95	0.35	0.06	0.00	0.18	0.00	1953.59	1961.14
8	0.23	0.12	0.08	0.17	0.23	0.00	12.86	13.68
9	412.28	12.33	0.98	0.88	1.03	0.00	0.00	427.49
10	22.24	0.40	0.19	0.38	0.46	0.10	0.92	24.70
11	1.29	2.27	0.33	0.50	0.63	0.13	0.72	5.87
12	0.00	15.07	0.51	0.60	0.77	0.16	0.00	17.10
13	10.68	394.42	15.62	4.47	7.98	0.00	1.91	435.08
14	10.28	2.67	0.72	2.21	0.00	0.08	1.99	17.95
15	0.00	0.94	0.29	1.38	0.53	0.25	0.42	3.82
17	0.41	2.31	46.56	0.00	1138.86	0.58	0.31	1189.02
18	0.09	0.19	0.56	3.72	45.63	0.66	0.13	50.99
19	0.00	2.27	38.78	0.00	0.00	0.61	0.00	41.65
20	0.00	0.00	6.84	5.05	183.58	3.36	0.00	198.84
21	0.00	0.00	2.31	36.27	9.29	26.08	0.00	73.96
22	0.04	0.00	0.98	16.22	3.89	0.00	0.00	21.13
23	0.03	0.00	0.35	1.60	0.52	94.61	0.00	97.10
24	0.00	0.00	0.14	0.40	0.32	0.00	0.00	0.86
25	0.81	7.71	522.38	0.00	149.44	0.00	0.11	680.45
26	0.18	0.36	20.97	3.92	1.44	0.35	0.00	27.22

APPENDIX D

Angular Dependence of Dosimeters

Multiple detectors were placed at 0, 30, 45, 60 and 90 degrees from an F-18 source. The results were corrected for a distance of one meter (distance correction) so that the exposures (raw data) could be compared.

0 degrees						***90 degrees***	
	raw data		***raw data***		***raw data***		***raw data***
detector no.	***(mrem)***	**detector no.**	***(mrem)***	**detector no.**	***(mrem)***	**detector no.**	***(mrem)***
1091	**70**	1113	**73**	1096	**70**	1112	**51**
1093	**72**	1111	**71**	1092	**71**	1103	**49**
1094	**71**	1108	**70**	1101	**69**		

30 degrees		**Distance**	***45 degrees***		**Distance**	***60 degrees***		**Distance**
	raw data	**Correction**		***raw data***	**Correction**		***raw data***	**Correction**
detector no.	***(mrem)***	(1 meter)	**detector no.**	***(mrem)***	(1 meter)	**detector no.**	***(mrem)***	(1 meter)
1107	**53**	70.09	1105	**39**	77.54	1097	**26**	104.00
1100	**49**	64.80	1099	**40**	79.52	1110	**25**	100.00
1109	**56**	74.06	1104	**35**	69.58	1106	**27**	108.00
1095	**56**	74.06	1114	**35**	69.58	1090	**25**	100.00

VITA

Name:	Audra Lee Coker
Address:	130 CR 310 Rosebud, TX 76570
Email Address:	saathoff_a@hotmail.com
Education:	B.S., Nuclear Engineering, Texas A&M University, 2005 M.S., Health Physics, Texas A&M University, 2007